
Article:
Green, J.E. orcid.org/0000-0001-9884-4954, Stone, D.A. orcid.org/0000-0002-5770-3917, Foster, M.P. et al. (1 more author) (2015) Spatially Resolved Measurements of Magnetic Fields Applied to Current Distribution Problems in Batteries. IEEE Transactions on Instrumentation and Measurement , 64 (4). pp. 951-958. ISSN 0018-9456

https://doi.org/10.1109/TIM.2014.2362432

Spatially Resolved Measurements of Magnetic Fields Applied to Current Distribution Problems in Batteries

James E. Green, David A. Stone, Martin Foster, and Alan Tennant, *Member, IEEE*

***Abstract*—This paper presents a novel instrumentation system for spatially resolved measurements of steady-state and slowly time varying magnetic fields. The instrumentation system has a measurement area of 400 mm by 200 mm consisting of 256 magnetic "pixels" each measuring the magnetic field crossing the centre of the pixel area as three orthogonal vectors. The specified minimum resolution of our chosen sensor is approximately 1.0×10^{-7} T and the maximum specified measurable magnetic field is 8.0×10^{-4} T. Magnetic field data can be recorded at approximately one frame per second.**

This paper also reports the application of this instrumentation system to measurements on lead acid batteries and hybridized battery ultra-capacitor combinations. The objective of this work is to infer, for the first time, the moving charge distribution inside the battery volume by measuring the magnetic field resulting from the moving charge. Empirical tests are reported which show the current distribution as a function of increasing distance down the plate away from the terminal is highly likely to be exponential in nature, with most current flowing in the uppermost portion of the battery.

***Index Terms*—Magnetic Field Measurement, Magneto-restive Sensor, Current Distribution, Biot-Savart, Inverse Problem.**

I. Introduction

THE design of the Planté flooded lead acid battery has been essentially unchanged for over a century. A lead lattice is filled with lead oxide forming the negative electrode and pure lead forming the positive electrode. The plates are spaced by insulators and immersed in an electrolyte of hydrogen sulfide [1]. The area of the positive plate is fundamental in determining the capacity and the condition of the plates is the main determiner of the battery's state of health (SoH) [2]; the present maximum capacity as a ratio of the nominal maximum capacity at the time of manufacture. The area of the plates governs to some degree the maximum peak discharge current [1]. Similar arguments apply to flat plate cells (where both electrodes are lattices and the H_2SO_4 is added to the PbO in the positive plate) and VRLA batteries (in which the electrolyte is a gel) and more generally to other battery technologies including Li^+. An ideal scenario for current flow in the battery is one in which each unit of plate area contributes equally to current flow, however this is not generally the case; the current flow in a standard lead acid battery is dominated by current flowing "across the top" – between the parts of the plates closest to the terminals.

Department of Electronic and Electrical Engineering, Sir Frederick Mappin Building, Mappin Street, Sheffield, S1 3JD, UK +44 (0)114 222 5847

This work was funded under EPSRC grant no. EP/H050221/1

Manuscript received October 14, 1066; revised August 26, 1789.

This work aims to observe experimentally the current distribution in a lead acid battery under constant current charge or discharge by measuring the magnetic field generated around the battery by the moving element of charge within it. This information may enable the design of new plate geometries which overcome or partially ameliorate some long standing problems in many battery chemistries including, for example, dynamic charge acceptance [3], [4].

The remainder of this paper is split in to eight sections. Section II presents a brief review of magnetic sensors. Section III provides a review of some existing magnetic field measurement systems. Section IV describes our measurement system and Section V describes our approach to validation. Results related to moving charge distribution and the associated discussion is presented in Section VI. Section VII reports results of magnetic field measurements of the connection of a battery and a ultracapacitor system. We noninvasively observe the charge redistribution between the ultracapacitors and battery after charge and discharge events. Sections VIII and IX provide a conclusion and our plans for future work.

II. Review of Magnetic Sensor Technologies

Several technologies exist for the detection of magnetic flux. The objective of this section is to briefly review the available technology to illuminate the choice of (magneto resistive) sensors for this application. A more exhaustive review of magnetic sensing technology is available elsewhere [5], [6].

There are a range of sensors commonly used for magnetometry including fibre-optic [7], [8], optically pumped [9], search-coil, nuclear precession, magneto-resistive, fluxgate, superconducting quantum interference devices (SQUIDs) magnetic tunnel junction, and Hall-effect sensors. The fibre-optic, optically pumped and nuclear precession devices are unsuitable in this application because a non-trivial amount of extra instrumentation is required to use these techniques making them impractical when several hundred magnetometers are required in a relatively confined space.

SQUIDs are superconducting devices and so must be cooled to cryogenic temperatures, making them impractical in this application. However several magnetic imaging systems have been produced using a mechanical raster scanning approach and a single sensor. Magnetic tunnel junctions (MTJs) are composed of two ferromagnetic magnetic materials separated by a thin a few tens of nanometers insulator. Under the influence of a magnetic field, electrons can quantum mechanically tunnel through the insulator [10]. These devices

are approximately the same order of magnitude in terms of device footprint as SQUIDs, several commercial examples are available for example Micro Magnetics, Inc. [1].

Fluxgates, which detect a field by observing the difference in current required to saturate a magnetic material in both positive and negative B field directions [11]–[18] are a suitable sensor for this application. They can be produced using a small (e.g. 15 mm) diameter toroidal supermalloy core while maintaining sufficient resolution for this work. The required instrumentation could be made such that the "pixel" size (including readout circuits) would be quite large, but not undesirably so compared to a standard SLI (starter, lights and ignition) battery. The main drawback is the cost of each sensor is presently approximately twenty times greater than a magneto-resistor based solution.

Magneto-resistors are easily integrated and have minimal instrumentation requirements. The Honeywell HMC5883L is a commercially available fully integrated 3 axis magnetometer housed in a 3 mm x 3 mm LLC package. It consists of the three orthogonal MR sensors, ADC converters and an integrated ASIC providing a rudimentary state machine which allows I^2C interfacing. It is designed for compassing applications in hand-held devices but is almost ideal for the present investigation. The main drawback of this chip is that every individual IC has the same hard-wired I^2C address. Consequently a system of bus switching and multiplexing is employed to allow addressing of all devices, this will be discussed in section IV

III. Review of Spatially Resolved Magnetic Field Measurement Systems

Several examples of spatially resolved magnetic field measurement systems exist in the literature including [19]–[31]. Several of these systems operate a single SQUID device and mechanically scan it across the area being imaged. Most ICs have an area less than $5\ \mathrm{cm}^2$, so can be scanned quickly even if the data acquisition rate of the system is limited due to mechanical considerations. Batteries are between one and three orders of magnitude larger in area than most IC headers. Scanning the battery surface is highly undesirable in this application as it will severely limit the frame rate. Several other systems which appear to follow from [32] and are based on scanning methods making use of magneto-resistive devices [33] and magnetic tunnel junctions [34], a commercial IC testing microscope is available from Micro Magnetics, Inc. [1] and is reported in [35]. Several other systems exist based on photonic crystals as a measurement sensor for example [36], [37] and also the work of Tsukada et al. in which an array of 64 SQUID devices are used to perform field imaging of a foetal heart in vivo [38]. Y. Terashima and I. Sasada [39] used a miniaturised flux-gate to detect the magnetic domains in a sheet of 3% GOSS. The flux-gate was stationary and the stage holding the sample was scanned under it. In a separate work by Tsukada [40], eddy currents have been imaged – although no effort was made to extract the current distribution from the field data. Tsukada's work was concerned with two dimensional non-destructive evaluation of sheet metal for aircraft fabrication using two orthogonal magneto-resistive sensors. The metal part under test is scanned under the stationary sensor by an x-y stage. Benitez et al. [41], [42] have produced a similarly structured magnetic field imaging system, but applied to finding hidden ferrous targets, for example reinforcements in concrete. Hofer [27] has investigated the internal structures of commercial MR sensors and contrinbuted to the inverse problem literature. Ny et al. [43] have performed similar work on fuel cells using punctual magnetic sensors.

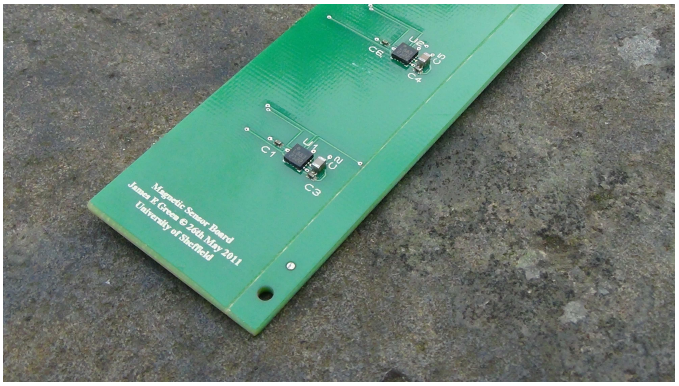

Fig. 1. A Honeywell HMC5883L magnetic sensor on a sensor column PCB; the sensor is 3 mm square. The copper tracking follows a manufacturer recommended layout [58] which minimises interference due to the small currents flowing in the copper traces.

The solution of the magnetic field to current distribution is a ill-posed inverse problem [44]–[54] which often has non-unique solutions. Several methods have been proposed to better represent these inverse problems including, [19], [55]–[57]. It will be shown shortly that the battery current distribution can, with some assumptions, also be reduced to a two dimensional Biot-Savart problem where a describing expression for the current distribution may be postulated and then empirically shown to be in good agreement with observation. A genetic algorithm may be used to search for the parameters of the describing equation and such an algorithm is in development. The next section of this paper is given over to a description of the measurement system.

IV. Experiment System Design

The magnetic field detection system is composed of a matrix of Honeywell HMC5883L magnetic sensors[2] mounted on PCBs as shown in Fig. 1. The measurement system is broken into two levels of hardware in which each "column" of sensors is on a separate PCB. The column PCBs plug into a backplane. The design is also divided into software/firmware and hardware elements.

Each sensor is composed of three orthogonal magneto-resistive elements combined with analogue to digital conversion and readout electronics packaged in a 3 mm x 3 mm LLC ASIC. Communication with each sensor is performed via an I^2C interface. The sensor design prohibits more than one

[1]Micro Magnetics, Inc. 617 Airport Road, Fall River, MA, 02720, USA.

[2]Honeywell M & P S, 12001 State Highway 55 Plymouth, MN 55441, USA.

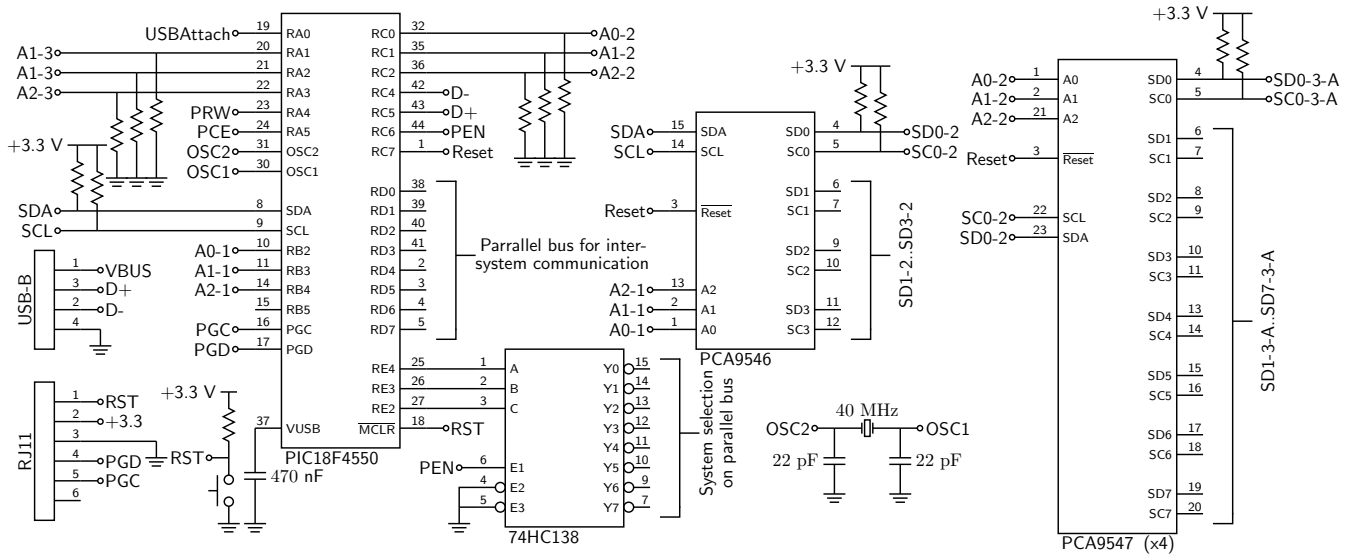

Fig. 2. A simplified circuit diagram of the magnetic field measurement system backplane board. A PC running bespoke acquisition software (C++ & Qt) connects to a PIC micro-controller via USB 2.0. The microcontroller also communicates with the sensors over I^2C which has three levels of multiplexing, 4:1, 8:1 (shown here) and a further 8:1 (shown in Fig.4) to permit the connection of 256 similarly addressed devices on a single bus. All resistors 2.2 kΩ.

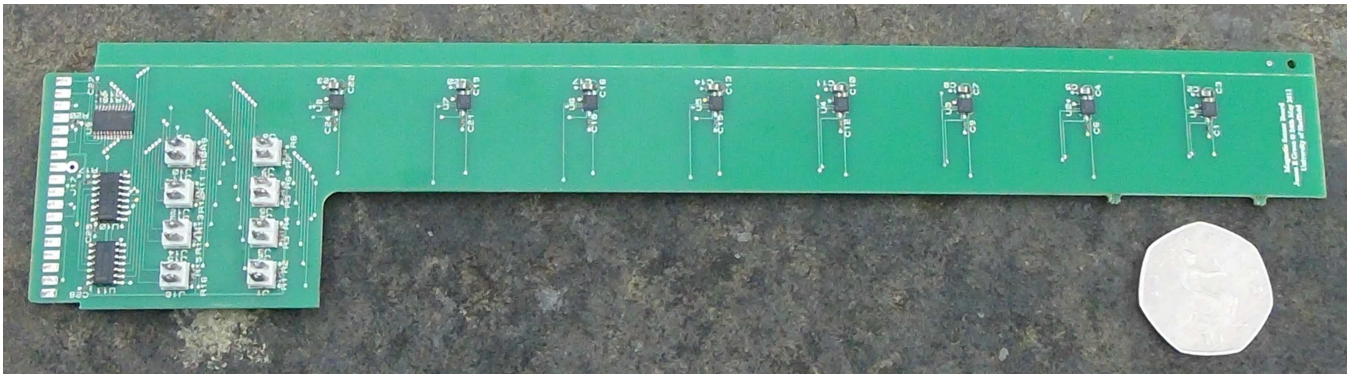

Fig. 3. A "column" board, one of 32 in the measurement system. The ICs next to the card edge contacts (far left) perform I^2C multiplexing and priority encoding. The connectors allow debugging of the I^2C bus at the individual sensor level. The 50 pence piece – for scale – is 27.3 mm in diameter.

device on an I^2C bus, a system of multiplexing and switching is used to overcome this limitation. The column PCB, shown in Fig. 3. is composed of eight individual sensors and associated interfacing components. The sensors are spaced 25.4 mm apart in the vertical direction. One level of bus multiplexing is also included on the column PCB. The simplified circuit diagram for the column PCB is shown in Fig. 4.

The sensors and interfacing electronics are controlled via the I^2C bus which operates at 400 kHz. The simplified circuit diagram for the backplane is shown in Fig. 2. It houses a further two levels of I^2C multiplexing and a micro-controller (Microchip PIC18F4550) running bespoke firmware. The microcontroller sends frame data via USB to a PC.

V. Experimental Validation

To test that the magnetic field detection system operates correctly the current in a long straight wire (Fig. 5) is measured and compared to the expected value determined by application of the Biot-Savart law (1) where μ_0 is the permeability of free space, I is the current flowing in the closed curve (wire), $d\mathbf{l}$

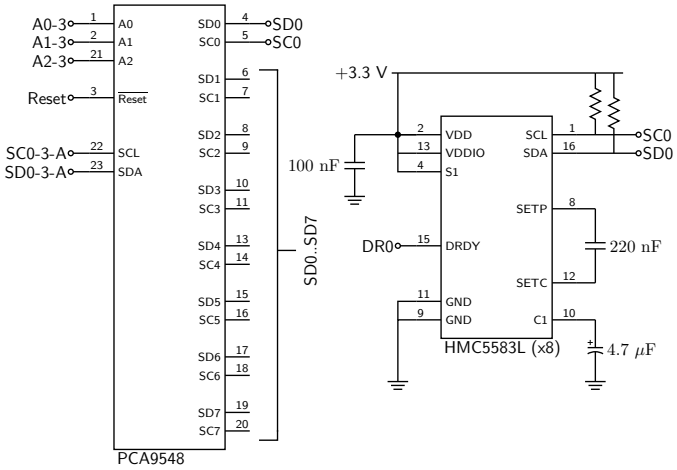

Fig. 4. A simplified schematic of a "column" circuit board. 8 HMC5883L sensors connect to the PCA9548 I^2C bus multiplexer. Priority encoding of the data ready (DR0..DR7) lines is not shown. There are 32 "column" boards in the system. All resistors 2.2 kΩ.

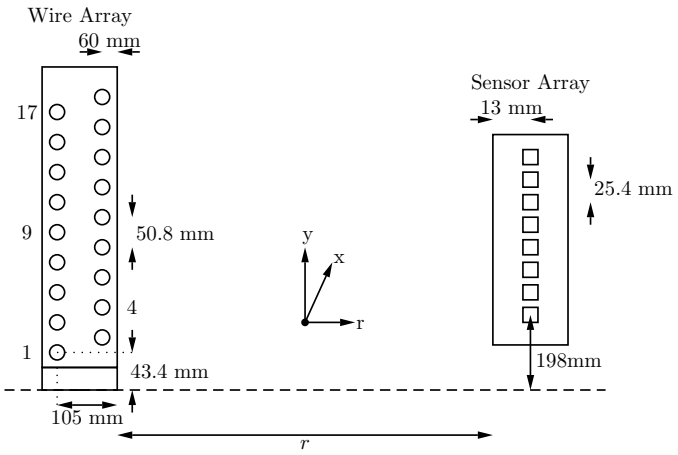

Fig. 5. A schematic diagram of the straight wire acceptance testing set-up. The copper pipe – straight wire – is supported by the wooden structure on the left and is axially aligned perpendicular to the page. A column sensor board is shown on the right. The vertical datum is represented by the dashed line.

is an infinitesimal length of the curve parallel to the direction of current flow, $\hat{\mathbf{r}}$ is the unit vector in the direction of the measurement position from the wire and $|\mathbf{r}|$ is the magnitude of the vector between the wire and measurement point.

$$B = \frac{\mu_0}{4\,\pi} \int_C \frac{I\,d\mathbf{l} \times \hat{\mathbf{r}}}{|\mathbf{r}|^2} \tag{1}$$

The Biot-Savart law can be reduced to (2) in the long straight wire case.

$$B = \frac{\mu_0\, I}{2\,\pi\,|\mathbf{r}|} \tag{2}$$

A diagram of the experimental validation test set-up is shown in Fig. 5. In Fig. 5 a wooden structure (left), which extends into the page, is shown with eighteen holes vertically spaced at 25.4 mm increments. A column PCB is shown to the right of Fig. 5 and relevant physical dimensions are labelled. A thin copper pipe, which is much longer than the length of the magnetic measurement array, extends into the page, held by the wooden frame. A DC current (approximately 3 A) is passed through the copper pipe and the resulting magnetic field is recorded by the system, having first nulled the earth's magnetic field. The nulling is achieved by taking a 'dark' frame prior to the test and subtracting it from all of the data frames which follow. Periodic recalibration is possible but has not been found necessary. Example data in which the copper pipe is in hole #10 and the distance r is 0 mm is shown in Fig. 6. Data has been gathered for $r = 0$ and 50.8 mm using holes #1, 4, 7, 10, 13, 16 & 18 and for r = 101.6, 152.4, 203.2 and 254 mm in holes #1, 10 and 18. This data is in good agreement with predictions obtained from (2).

VI. Magnetic field measurement of Batteries and Current Distribution Extraction

The examination of batteries using the measurement system is superficially similar to the long straight wire problem. However the current is no longer confined and the battery cannot be reduced to a single wire analogue. A number of assumptions may be made.

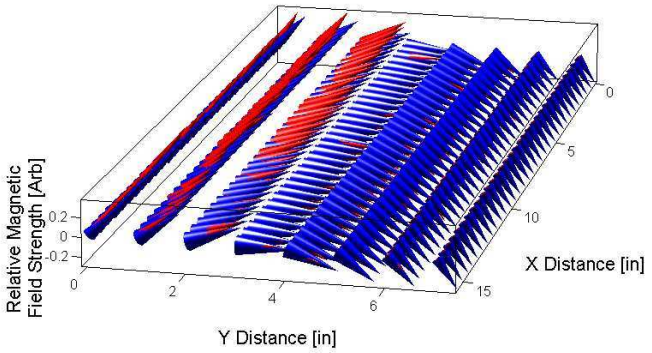

Fig. 6. Magnetic field data from a long straight wire in hole # 10 and $r = 0$ mm. The size of the cones represents relative field magnitude. Conventional current flows away from the reader, into the page. The magnitude and direction of the measured magnetic field (red) agrees well with calculation (blue).

1) The measured field is dominated by the current flowing in the parts of the battery which are closest to the measurement system. This does not represent a very great loss of accuracy because field varies with distance squared. Generally the internal construction of the battery varies little as distance normal to the measurement plane increases.
2) The dominant direction of current flow in the battery will be horizontally across the battery.
3) The current flowing between the plates is uniformly distributed across the width of the plate (the dimension normal to the plane of the measurement).
4) Since the current flowing in the plate is only a function of the vertical distance from the battery terminals the width of the battery may be dispensed with.

Using these assumptions the battery may be modelled by a number of straight wires carrying a varying current and is therefore described by a number of Biot-Savart expressions. To facilitate testing, this model may be physically realised by a printed circuit board and is shown on the left of Fig. 7.

The battery examined in this paper is the Furukowa FTZ12-HEV [59], [60]. Initially, an itterative approach was adopted to find the resistances required to cause, as nearly as possible, identical fields from the PCB and the real battery. After several iterations it became clear that a well-defined exponential relationship (3) exists between wire current and distance from the top of the plate.

$$I_n = I_0 \exp\left(-k\,n\,d_w\right) \tag{3}$$

Where I_0 is the current in the zeroth wire, closest to the battery terminals, k is a fitting coefficient, n is the present wire number and d_w is the inter-wire distance. The integral of (3) must equal the total current flowing in the PCB battery and in the real battery. This equivalence relies on accurate measurement of d, the distance from the edge of the battery plates to the measurement system. Since the battery is encased in plastic, d is estimated. The result of fitting is shown in Fig. 8. The dominant region of current flow is shown by the greatest change in direction between adjacent cones. The Furukowa battery (red) shows some z-axis components around

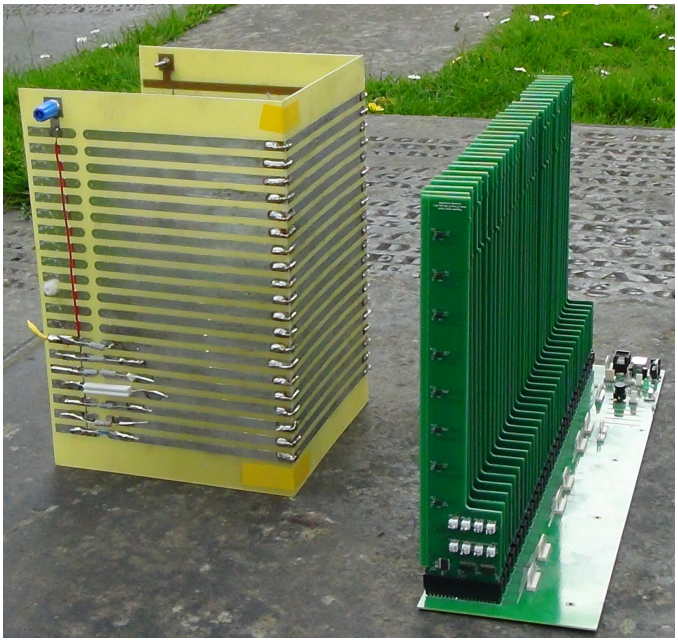

Fig. 7. The magnetic field measurement system and PCB 'battery' shown for the purpose of illustrating the physical test layout.

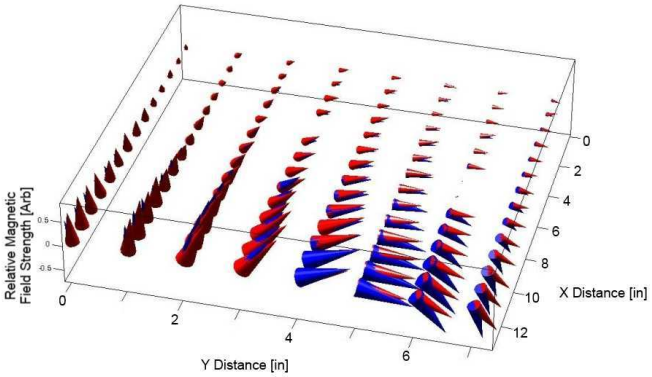

Fig. 8. A half field (cut along y axis near to the centre of the battery and PCB 'battery'). The real battery measurement (red) and PCB 'battery' measurement (blue) in which each of the traces in the PCB carry an exponentially decreasing current match quite well in terms of magnetic field magnitude and direction, even towards the outer regions of the measurement area.

rows 10, 12 and 14 which is not apparent in the PCB battery. This is because the PCB battery trace spacing makes it slightly taller than the Furukowa battery's active area, consequently the field curvature which is due to current flowing orthogonally (away from or towards) the plane of the sensors is positioned slightly incorrectly in the magnetic field plot. The orthogonal current flow is caused by the batteries non-zero plate width and the fact that the terminals are positioned farthest from the plane of the magnetic sensors. This is necessary to avoid undue influence on the measurement of the field created by the battery current as it flows away from and towards the battery in the connecting wires.

A simple physical explanation for the the exponential distribution of the current as a function of vertical distance from the battery terminals is highly desirable. Assume that,

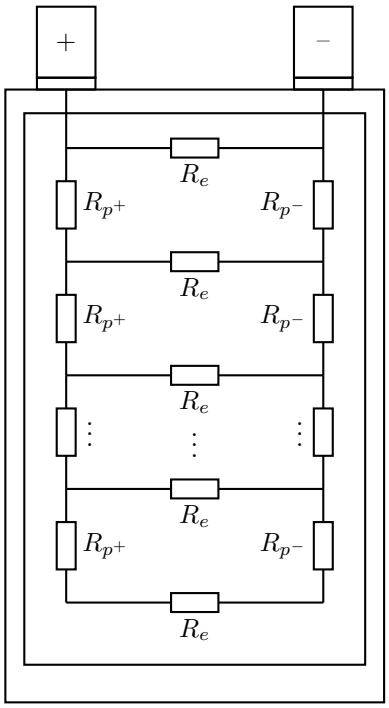

Fig. 9. A two plate battery in which the plates are ascribed an incremental resistance, R_{p^+} and R_{p^-} which will be constant assuming the plates are homogeneous and have constant thickness and width as a function of height. Similarly, assuming the electrolyte is homogeneous a constant incremental resistance, R_e, may be applied to it.

1) The battery consists of only two plates separated by an electrolyte. This simplifies visualisation of the problem only and does not represent a loss of generality over a parallel plate battery consisting of many cells in series.
2) The plates are negligibly thick compared to their width and height.
3) The plates have constant resistivity per unit volume.

These assumptions are true for a wide range of lead acid batteries and they allow the development of the model shown in Fig. 9 in which R_e is a resistance representing a small region of the electrolyte and R_{p^+} is a resistance representing a small region of the more positive plate and n is an integer. Similarly R_{p^-} is a resistance representing a small region of the more negative plate.

It is trivial to show that the current flowing in each R_e is exponentially related to the relative values of R_e and $(R_{p^-} + R_{p^+})$ and the position of the particular R_e under consideration in the ladder.

VII. Battery System Monitoring

The magnetic field measurement system has been applied to a simple battery and ultracapacitor system which is composed of a Yuasa YTZ10S 8.5 Ah battery in parallel with a series connection of six ultracapacitors (Maxwell PowerCache PC2500 2.7 V_{max} 2500 F) having equivalent capacitance of 416 F. The parallel combination of battery and ultracapacitors are charged and discharged by a battery cycling system which finds general use in energy storage research at Sheffield. The objective is to attempt to record a series of frames of magnetic

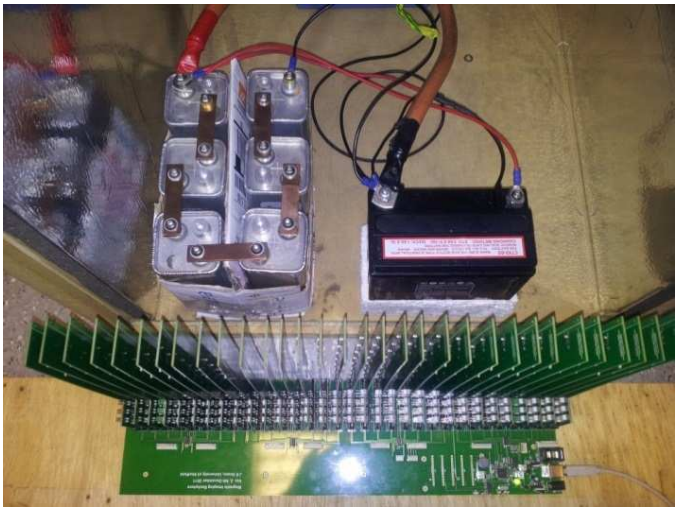

Fig. 10. left: Ultracapacitor bank. right: AGM Battery (on a 50 mm polystyrene block). Details given in Section VII.

field data and assemble them into a magnetic movie showing the transient charge redistribution which occurs between the battery and ultracapacitor bank at the end of charging and discharging events. To show the application of the measurement system in a transient situation. This experiment is a simple example of non-invasive battery system monitoring. The test set-up is shown in Fig. 10.

The data acquired is available in MPEG format [61]. Assuming charging takes place the expected result is that the battery dv/dt will be lower because it has higher capacity and because the electrochemical processes are non-linear. Whereas the capacitor voltage will follow the integral of current in proportion to capacitance $V = \frac{1}{C} \int I(t)\,\mathrm{d}t$. After the charging period ends and the current external to the battery – ultracapacitor system falls to zero a circulating current exists which acts to equalise the voltage on the ultracapacitors and the battery. The magnetic field due to this circulating current has been unambiguously measured. The data is somewhat difficult to analyse however because the shape of the ultracapacitor bank is such that there are large components of magnetic field generated due to current flowing in the copper bus bars perpendicular to the measurement plane. Moreover the field due to the current in the ultracapacitors appears to be dominated by the field due to the current in the closest copper bus bar. The three dimensional nature of the problem cannot be escaped without either smaller ultracapacitors or a larger measurement plane in front of which the capacitor bank can be unfolded into a line of capacitors where the dominant current flow is parallel to the plane of the measurement.

VIII. Conclusion

This paper has reported the novel application of a magnetic field imaging instrument capable of recording one frame of three axis magnetic data per second on a single plane of 256 sensors arranged in 32 rows of 8 magnetic "pixels". The measurement system is comparable in sensitivity to the recent system after Le Ny et al. [43], but having more sensors, and aproximately an order of magnitude lower sensitivity than the 1-D system of Benitez et al. [42]. The measurement system has been verified on a series of long wire (Biot-Savart) problems which yield results comparable with theory. The measurement system has been applied to a steady state battery charging problem. The current distribution in the battery has been closely approximated in two dimensions by an exponential function of distance down the plate away from the terminal. It has been postulated that the exponential distribution of current away from the terminal results from the constant resistance per unit volume of the plate. A simple circuit model has been used to show that the measured result is consistent with some reasonable assumptions including a constant plate resistance per unit volume. A series of straight wires etched onto a PCB have been used to experimentally model the battery current distribution and have confirmed that an exponential current distribution produced a magnetic field very similar to that observed in the real battery. This self-consistency does not preclude the possibility of other current distributions producing the same result, however the description of the battery as a series of incremental resistances which yields a very similar exponential distribution provides us with considerable confidence in this key result. The current distribution coefficients resulting from this work were arrived at by empirically by an iterative approach. The development of a genetic algorithm to extract the coefficients of the current distribution equation is in progress.

The measurement system was used to record a transient event at one frame per second – the equalisation of charge between a series connection of ultracapacitors and a standard lead acid battery after a period of charging. The circulating current equalising the capacitor bank and battery was clearly observed over a period of ten seconds.

IX. Future Work

A primary problem of this measurement system lies in the addressing structure of the array of magnetic sensors. The chosen multiplexing structure has limited the frame rate to approximately two orders of magnitude lower than the maximum data rate of an individual sensor. The development of this measurement system is on-going and a higher frame rate is highly desirable to capture transient events for example (switch-over in a UPS system or peak current transients at the initialisation of regenerative breaking in electric vehicle applications) with high fidelity.

A second less tractable problem is that the battery has to be connected to a power electronics system with wires and the field from the wires influences to some degree the field ascribed to the battery. This is ameliorated somewhat in practice by the physical arrangement of the battery and the measurement system. This practical set-up relies on the r^2 term to make the contribution from the wire negligible compared to the battery which is much closer to the measurement system.

References

[1] D. Linden and T. Reddy, *Handbook of Batteries*, 3rd ed. McGraw-Hill Professional, 2001.

[2] T. R. Crompton, *Battery Reference Book*, 3rd ed. Newnes, 2000.

[3] J. Kowal, D. Schulte, D. U. Sauer, and E. Karden, "Simulation of the current distribution in lead-acid batteries to investigate the dynamic charge acceptance in flooded SLI batteries," *7th International Conference on Lead-Acid Batteries, Journal of Power Sources*, vol. 191, pp. 42–50, Jun. 2008.

[4] E. Karden, S. Ploumen, B. Fricke, T. Miller, and K. Snyder, "Energy storage devices for future hybrid electric vehicles," *Journal of Power Sources*, vol. 168, no. 1, pp. 2 – 11, 2007.

[5] J. G. Webster, *The Measurement, Instrumentation, and Sensors: Handbook*, ser. Electrical engineering handbook series. CRC Press, 1999.

[6] D. Robbes, "Highly sensitive magnetometers – a review," *Sensors and Actuators A: Physical*, vol. 129, no. 12, pp. 86 – 93, 2006.

[7] J. E. Lenz, C. D. Anderson, and L. K. Strandjord, "Magnetic materials characterization using a fiber optic magnetometer," *Journal of Applied Physics*, vol. 57, no. 8, pp. 3820–3822, 1985.

[8] M. Shahinpoor, S. G. Popa, and L. O. Sillerud, "Smart fiber optic magnetometer," United States of America Patent 6 433 543, Aug., 2002.

[9] W. Farthing and W. C. Folz, "Rubidium vapor magnetometer for near earth orbiting spacecraft," *Review of Scientific Instruments*, vol. 38, no. 8, pp. 1023–1030, 1967.

[10] M. E. Eames and J. C. Inkson, "Interface scattering and the tunneling magnetoresistance of Fe(001)/MgO(001)/Fe(001) junctions," *Applied Physics Letters*, vol. 88, no. 25, pp. 252 511–252 511–3, 2006.

[11] P. Ripka, "Advances in fluxgate sensors," *Sensors and Actuators A: Physical*, vol. 106, no. 1–3, pp. 8 – 14, 2003, proceedings of the 4th European Magnetic Sensors and Actuators Conference.

[12] M. Djamal and R. N. Setiadi, "Development of fluxgate magnetometer using double cores probe," in *Industrial Electronics, 2009. ISIE 2009. IEEE International Symposium on*, 2009, pp. 138–142.

[13] W. S. Watson, "Single core triaxial flux-gate magnetometer," United States of America Patent 5 270 648, Dec., 1993.

[14] P. Ripka, "New directions in fluxgate sensors," *Journal of Magnetism and Magnetic Materials*, vol. 215–216, no. 0, pp. 735–739, 2000.

[15] H. Trujillo, J. Cruz, M. Rivero, and M. Barrios, "Analysis of the fluxgate response through a simple SPICE model," *Sensors and Actuators A: Physical*, vol. 75, no. 1, pp. 1–7, 1999.

[16] P. Ripka, *Magnetic Sensors and Magnetometers*. Artech House, 2000.

[17] A. Baschirotto, E. Dallago, P. Malcovati, M. Marchesi, and G. Venchi, "A fluxgate magnetic sensor: From PCB to micro-integrated technology," *Instrumentation and Measurement, IEEE Transactions on*, vol. 56, no. 1, pp. 25 – 31, Feb. 2007.

[18] A. Baschirotto, E. Dallago, P. Malcovati, M. Marchesi, E. Melissano, M. Morelli, P. Siciliano, and G. Venchi, "An integrated micro-fluxgate magnetic sensor with front-end circuitry," *Instrumentation and Measurement, IEEE Transactions on*, vol. 58, no. 9, pp. 3269–3275, Sep. 2009.

[19] P. Pesikan, M. L. G. Joy, G. Scott, and R. Henkelman, "Two-dimensional current density imaging," *Instrumentation and Measurement, IEEE Transactions on*, vol. 39, no. 6, pp. 1048–1053, Dec 1990.

[20] J. R. Kirtley, M. B. Ketchen, K. G. Stawiasz, J. Z. Sun, W. J. Gallagher, S. H. Blanton, and S. J. Wind, "High–resolution scanning SQUID microscope," *Applied Physics Letters*, vol. 66, no. 9, pp. 1138–1140, 1995.

[21] J. E. Mcfee, R. Ellingson, J. Elliott, and Y. Das, "A magnetometer system to estimate location and size of long, horizontal ferrous rods," *Instrumentation and Measurement, IEEE Transactions on*, vol. 45, no. 1, pp. 153–158, Feb 1996.

[22] L. Knauss, A. Cawthorne, N. Lettsome, S. Kelly, S. Chatraphorn, E. Fleet, F. Wellstood, and W. Vanderlinde, "Scanning SQUID microscopy for current imaging," *Microelectronics Reliability*, vol. 41, no. 8, pp. 1211 – 1229, 2001.

[23] S. Chatraphorn, E. F. Fleet, F. C. Wellstood, L. A. Knauss, and T. M. Eiles, "Scanning squid microscopy of integrated circuits," *Applied Physics Letters*, vol. 76, no. 16, pp. 2304–2306, 2000.

[24] C. Teo, H. Lwin, V. Narang, and J. M. Chin, "Device-level fault isolation of advanced flip-chip devices using scanning squid microscopy," in *Physical and Failure Analysis of Integrated Circuits, 2008. IPFA 2008. 15th International Symposium on the*, 2008, pp. 1–4.

[25] D. P. Vallett, "Scanning squid microscopy for die level fault isolation," in *ISTFA 2002: 28th International Symposium for Testing and Failure Analysis*, Nov. 2002, pp. 391–396.

[26] L. A. Knauss, B. M. Frazier, H. M. Christen, S. D. Silliman, K. S. Harshavardhan, E. F. Fleet, F. C. Wellstood, M. Mahanpour, and A. Ghaemmaghami, "Detecting power shorts from front and backside of IC packages using scanning squid microscopy," in *ISTFA 1999: 25th International Symposium for Testing and Failure Analysis*, Nov. 1999, pp. 11–16.

[27] D. Hofer, T. Wiesner, and B. Zagar, "Analyzing 2D current distributions by magnetic field measurements," in *Instrumentation and Measurement Technology Conference (I2MTC), 2012 IEEE International*, May 2012, pp. 2061 – 2066.

[28] I. Marinova, H. Endo, S. Hayano, and Y. Saito, "Inverse electromagnetic problems by field visualization," *Magnetics, IEEE Transactions on*, vol. 40, no. 2, pp. 1088–1093, March 2004.

[29] E. Nativel, T. Talbert, T. Martire, C. Joubert, N. Daude, and P. Falgayrettes, "Near-field electromagnetic tomography applied to current density reconstruction in metallized capacitors," *Power Electronics, IEEE Transactions on*, vol. 20, no. 1, pp. 11–16, Jan 2005.

[30] P. Holzl and B. Zagar, "Deconvolution of high-resolution magnetic field scans for improved current density imaging," *Magnetics, IEEE Transactions on*, vol. 50, no. 2, pp. 101–104, Feb 2014.

[31] M. Lassahn and G. Trenkler, "A multi-channel magnetometer for field structure measurement based on time encoded flux-gate sensors," *Instrumentation and Measurement, IEEE Transactions on*, vol. 42, no. 2, pp. 635–639, Apr 1993.

[32] J. H. Wandass, J. S. Murday, and R. J. Colton, "Magnetic field sensing with magnetostrictive materials using a tunneling tip detector," *Sensors and Actuators*, vol. 19, no. 3, pp. 211–225, 1989.

[33] B. Schrag, X. Liu, M. Carter, and G. Xiao, "Scanning magnetoresistive microscopy for die-level sub-micron current density mapping," in *Physical and Failure Analysis of Integrated Circuits, 2004. IPFA 2004. Proceedings of the 11th International Symposium on the*, 2004, pp. 2–5.

[34] B. D. Schrag, M. J. Carter, L. X., H. J. S., and X. G., "Magnetic current imaging with magnetic tunnel junction sensors: Case study and analysis," in *International Symposium for Testing and Failure Analysis*, vol. 32, 2006, pp. 13–19.

[35] B. D. Schrag, X. Liu, J. S. Hoftun, P. L. Klinger, T. Levin, and D. P. Vallett, "Quantitative analysis and depth measurement via magnetic field imaging," *Electronic Device Failure Analysis*, vol. 7, no. 4, pp. 24–31, Nov. 2005.

[36] M. Vasiliev, V. Kotov, K. Alameh, V. Belotelov, and A. Zvezdin, "Novel magnetic photonic crystal structures for magnetic field sensors and visualizers," *Magnetics, IEEE Transactions on*, vol. 44, no. 3, pp. 323–328, 2008.

[37] M. Vasiliev, K. E. Alameh, and V. Kotov, "Magnetic field sensors and visualizers using magnetic photonic crystals," *Proc. SPIE*, vol. 7004, pp. 70 045D–70 045D–4, 2008.

[38] K. Tsukada, H. Sasabuchi, and T. Mitsui, "Measuring technology for cardiac magneto-field using ultra-sensitive magnetic sensor," *Hitach Review*, vol. 48, pp. 116–118, 1999.

[39] Y. Terashima and I. Sasada, "Magnetic domain imaging using orthogonal fluxgate probes," *Journal of Applied Physics*, vol. 91, no. 10, pp. 8888–8890, 2002.

[40] K. Tsukada, T. Kiwa, T. Kawata, and Y. Ishihara, "Low-frequency eddy current imaging using MR sensor detecting tangential magnetic field components for nondestructive evaluation," *Magnetics, IEEE Transactions on*, vol. 42, no. 10, pp. 3315–3317, 2006.

[41] S. Quek, D. Benitez, P. Gaydecki, and V. Torres, "Modeling studies on the development of a system for real-time magnetic-field imaging of steel reinforcing bars embedded within reinforced concrete," *Instrumentation and Measurement, IEEE Transactions on*, vol. 57, no. 3, pp. 571–576, March 2008.

[42] D. Benitez, S. Quek, P. Gaydecki, and V. Torres, "A 1-D solid-state-sensor-based array system for magnetic field imaging of steel reinforcing bars embedded within reinforced concrete," *Instrumentation and Measurement, IEEE Transactions on*, vol. 58, no. 9, pp. 3335–3340, Sep. 2009.

[43] M. Le Ny, O. Chadebec, G. Cauffet, J.-M. Dedulle, Y. Bultel, S. Rosini, Y. Fourneron, and P. Kuo-Peng, "Current distribution identification in fuel cell stacks from external magnetic field measurements," *Magnetics, IEEE Transactions on*, vol. 49, no. 5, pp. 1925–1928, May 2013.

[44] R. Kress, L. Kühn, and R. Potthast, "Reconstruction of a current distribution from its magnetic field," *Inverse Problems*, vol. 18, no. 4, p. 1127, 2002.

[45] R. Potthast and M. Wannert, "Uniqueness of current reconstructions for magnetic tomography in multilayer devices," *SIAM Journal on Applied Mathematics*, vol. 70, no. 2, p. 563, 2009.

[46] F. Yaman, V. G. Yakhno, and R. Potthast, "A survey on inverse problems for applied sciences," *Mathematical Problems in Engineering*, vol. 2013, no. 976837, pp. 1–19, 2013.

[47] H. Brauer, J. Haueisen, and M. Ziolkowski, "Verification of magnetic field tomography inverse problem solutions using physical phantoms," in *Computational Electromagnetics (CEM), 2006 6th International Conference on*, Apr. 2006, pp. 1 – 2.

[48] C. A. Borghi and M. Fabbri, "A combined technique for the global optimization of the inverse electromagnetic problem solution," *Magnetics, IEEE Transactions on*, vol. 33, no. 2, pp. 1947–1950, Mar 1997.
[49] L. Ghezzi, D. Piva, and L. Di Rienzo, "Current density reconstruction in vacuum arcs by inverting magnetic field data," *Magnetics, IEEE Transactions on*, vol. 48, no. 8, pp. 2324–2333, Aug 2012.
[50] T. Talbert, L. Nativel, T. Martir, S. Faucher, C. Joubert, and N. Daud, "Application of inverse problems to current density reconstruction inside components," *Applied Physics Letters*, vol. 86, no. 4, 2005.
[51] S. Begot, E. Voisin, P. Hiebel, E. Artioukhine, and J.-M. Kauffmann, "D-optimal experimental design applied to a linear magnetostatic inverse problem," *Magnetics, IEEE Transactions on*, vol. 38, no. 2, pp. 1065–1068, Mar 2002.
[52] T. Doi, S. Hayano, and Y. Saito, "Wavelet solution of the inverse source problems," *Magnetics, IEEE Transactions on*, vol. 33, no. 2, pp. 1935–1938, Mar 1997.
[53] L. Di Donato, I. Catapano, F. Soldovieri, and L. Crocco, "Imaging of 3D magnetic targets from multiview multistatic GPR data," in *Ground Penetrating Radar (GPR), 2010 13th International Conference on*, Jun. 2010, pp. 1 – 6.
[54] R. Ferrero, M. Marracci, and B. Tellini, "Uncertainty analysis of local and integral methods for current distribution measurements," *Instrumentation and Measurement, IEEE Transactions on*, vol. 62, no. 1, pp. 177–184, Jan 2013.
[55] H. Endo, T. Takagi, and Y. Saito, "A new current dipole model satisfying current continuity for inverse magnetic field source problems," *Magnetics, IEEE Transactions on*, vol. 41, no. 5, pp. 1748 – 1751, May 2005.
[56] G. Krukowski, S. Gratkowski, and R. Sikora, "Imaging of two-dimensional current density distributions from their magnetic field," in *Computer Engineering in Applied Electromagnetism*, S. Wiak, A. Krawczyk, and M. Trlep, Eds. Springer Netherlands, 2005, pp. 71–76.
[57] C. Wu and J. Xiao, "Electric current source estimation by high-res magnetic field restoration from sparse magnetic measurements," in *Signal Processing (ICSP), 2012 IEEE 11th International Conference on*, vol. 1, Oct 2012, pp. 299–302.
[58] Honeywell Aerospace, "HMC5883L 3-axis digital compass IC, form 900405 rev d," Mar. 2011. [Online]. Available: www.honeywell.com/magneticsensors
[59] L. Lam, N. Haigh, C. Phyland, and D. Rand, "High performance energy storage devices," United States of America Patent 8 232 006, Jul. 31, 2012.
[60] ——, "High performance energy storage devices," United States of America Patent 7 923 151, Apr. 12, 2011.
[61] J. E. Green, "Battery magnetic imaging project website." [Online]. Available: http://james-green.staff.shef.ac.uk/index.php?cont=magimage&head=2&foot=1

James E. Green James was born in London, England in 1985. He received the degrees of B.Eng, MSc and PhD in Electronic Engineering from the University of Sheffield, England in 2006, 2007 and 2012 respectively. His doctoral studies were with the Semiconductor Materials and Devices Group at Sheffield and concerned the development of novel instrumentation systems for characterisation of excess avalanche multiplication noise in silicon and 4H-Silicon Carbide and the determination of impact ionisation coefficients.

His principle interests are in the area of circuits, instrumentation, signal recovery and power electronic systems and devices specifically in new materials. Dr. Green is a lecturer at Sheffield University presently working on electronic systems design in several areas including optoelectroinc semiconductor characterisation, medical instrumentation, systems related to three dimensional spatially resolved transient magnetic field imaging in lead acid / ultra capacitor hybrid batteries, instrumentation and drive design for the optimisation of SR machines and problems in industrial microwave heating.

Martin P. Foster Martin P. Foster received the B.Eng. degree in Electronic and Electrical Engineering, the M.Sc.(Eng.) degree in Control Systems, and awarded a PhD for his thesis "Analysis and Design of High-order Resonant Power Converters from the University of Sheffield, Sheffield, U.K., in 1998, 2000, and 2003, respectively. In 2003 he became a member of academic staff at Sheffield specialising in power electronic systems and was made Senior Lecturer in 2010.

His current research interests include the modelling and control of power electronic converters with a focus on resonant power supplies and multilevel converters, battery management systems including charge/health estimation, grid connected energy storage, piezoelectric transformers, power electronic packaging and thermal management.

Alan Tennant Alan Tennant (M'92) received a B.Eng degree in electronic engineering and a Ph.D. degree in microwave engineering from the University of Sheffield, Sheffield, U.K., in 1985 and 1992, respectively.

Previously, he was with BAE Systems, Stevenage. He then joined DERA where he worked on phased array antenna systems before taking up an academic post at Hull University. He returned to Sheffield University in 2001 as a Senior Lecturer in the Communications and Radar Group where he is involved in research into techniques, materials and signal processing for adaptive radar signature management, novel three-dimensional phased array antenna topologies, acoustic array systems, and new research into time-modulated array antennas. He has published over 100 academic papers including several invited papers on adaptive stealth technology. His research has attracted substantial funding from both industry and government sources.

David A. Stone Dave was appointed into the Electrical Machines and Drives research group at the University of Sheffield in 1989 to expand the group into the area of power electronics and machine drives, and is heavily involved in EV / HEV research, together with power electronic energy conversion.

He has been involved in battery testing and management for over 10 years, being principle investigator on a number of industrially oriented projects such as INMOVE (EU funded with Mannesmann Sachs), Rholab (DTI funded with ALABC, Hawker batteries), ISOLAB42 (DTI funded with ALABC, FIAM, Exide), together with more academic work funded by the EPSRC, and direct industrial interaction with both battery and transport companies, together with projects not directly linked to battery technology, Prof. Stone has published approximately 150 papers including significant contributions in the areas of energy storage, resonant power converters and induction heating.